



Dalton
Transactions

**Bimetallic MOF-templated synthesis of alloy nanoparticles-
embedded porous carbons for oxygen evolution and
reduction reactions**

Journal:	<i>Dalton Transactions</i>
Manuscript ID	DT-ART-07-2019-002943.R1
Article Type:	Paper
Date Submitted by the Author:	20-Aug-2019
Complete List of Authors:	Zakary, Lionet; Osaka Prefecture University, Department of Applied Chemistry, Graduate School of Engineering Nishijima, Shun; Osaka Prefecture University Kim, Tae-Ho; Sun Moon University, Research Center for Eco Multi-Functional Nano Materials Horiuchi, Yu; Osaka Prefecture University, Department of Applied Chemistry, Graduate School of Engineering Lee, Soo; Sun Moon University, Department of Materials Engineering MATSUOKA, Masaya; Osaka Prefecture University,

SCHOLARONE™
Manuscripts

ARTICLE

Bimetallic MOF-templated synthesis of alloy nanoparticles-embedded porous carbons for oxygen evolution and reduction reactions

Received 00th January 20xx,
Accepted 00th January 20xx

DOI: 10.1039/x0xx00000x

Zakary Lionet^[a], Shun Nishijima^[a], Tae-Ho Kim^[b], Yu Horiuchi^{*[a]}, Soo Wahn Lee^[c] and Masaya Matsuoka^{*[a]}

Pyrolysis of metal–organic frameworks (MOFs) to produce metal nanoparticles embedded inside porous carbon matrix (M@PC) has drawn a lot of attention in recent years. Notably, Fe nanoparticles trapped in carbon matrix (Fe@PC) have been reported to efficiently promote oxygen evolution and reduction reactions (OER/ORR). However, research on the effect of doping on Fe particles has been scarce because of the difficulty to synthesize alloy of small size at elevated temperature. Herein, we focused on the development of bimetallic MOFs composed of Fe and a second metal M (M = Cr, Ni, Co, Mn) made from preassembled cluster and their sacrificial use to synthesis FeM@PC composites. After optimising the pyrolysis conditions and determining the optimal structure of MOF template, the materials were applied to electrocatalytic OER and ORR in 0.1 M KOH aqueous solution. Results showed that Co-Fe alloy composites exhibited the best activity for OER with a 210 mV cathodic shift to achieve 10 mA cm⁻² compared to pure Fe@PC. On the other hand, oxygen reduction reaction most efficiently proceeded on the Mn-Fe alloy composite, showing a 80 mV anodic shift in comparison to all other doped materials.

Introduction

Research on electrocatalysts for water splitting has greatly accelerated in recent years.¹ In earlier days, noble metal-based materials prevailed in this chemistry with Pt, Ru and Ir-based compounds reigning at the top.^{2–5} But recently, the development of electrodes made from abundant, non-toxic and cheap chemicals displaying high activity has become necessary to solve the deadlock over industrial water splitting.^{6–8} Carbon-based materials have been lately considered as attractive materials for oxygen evolution reaction (OER) and water reduction reactions due to their high activity at all pHs and excellent stability in aqueous media.⁹ Moreover, doping with heteroatoms or encapsulating metals

have been recognized as promising method to increase their efficiency.^{10–12}

Focus has been given on inorganic-organic hybrid composites to construct such metal-doped carbons materials through pyrolysis under inert gas owing to their features as unique precursors originating from their structure composed of organic and inorganic components intertwined at the molecular level. Among those materials, Metal–organic frameworks (MOFs), born from the coordination of organic linkers and inorganic metal clusters, also called Secondary-Building Units (SBUs), are extremely good candidate since they have benefits of inherent highly ordered structure formed via self-assembly and framework designability which enable them to possess at pristine state all the precursor elements needed to trigger the formation of desired metal-doped carbons. Eventually, pyrolysis of MOFs turned out to be a facile process to fabricate metal nanoparticles-embedded porous carbon materials (M@PC).^{13–15} MOFs-derived materials with nanocage,^{16,17} nanotube,^{18,19} bubble²⁰ and sphere^{21,22} structure have already been published. Among those reports, thermal treatment of iron-based MOFs to prepare Fe⁰, Fe₃C or Fe₃O₄ nanoparticles inside porous carbons was reported for WOR,²³ oxygen reduction reaction^{24,25} (ORR), adsorption²⁶ and storage²⁷ applications. Nonetheless, understanding of the crystalline and elemental structures of the parent-MOF onto the derivative M@PC morphology and activity is still shallow since few studies have been published.^{28,29} A deeper

[a] Department of Applied Chemistry, Graduate school of engineering
Osaka Prefecture University
1-1, Gakuen-cho, Naka-ku, Sakai, Osaka 599-8531, Japan
E-mail: matsumac@chem.osakafu-u.ac.jp
horiuchi@chem.osakafu-u.ac.jp

[b] Division of Mechanics and ICT Convergence Engineering, Sun Moon University,
Asan, Republic of Korea

[c] Department of Environmental and Bio-Chemical Engineering, Sun Moon
University, GalSan-Ri, Tangjung-Myon, Asan, Chung-nam 336708, Republic of
Korea

Electronic Supplementary Information (ESI) available: [details of any
supplementary information available should be included here]. See
DOI: 10.1039/x0xx00000x

comprehension should be indispensable for the creation of better catalysts.

On the other hand, alloying strategy for the embedded metal nanoparticles has been known as an efficient method to increase their chemical activity^{30,31}; however, their synthesis at nano-size on carbon support has been considered as a difficult process because alloying already deposited metals induced sintering and simply mixing precursors would create multiphase structures. As a precursor of alloy nanoparticles, the utilization of metal clusters in MOFs whose elemental compositions can be well controlled will effect a solution to these issues. For example, trinuclear iron clusters, typical iron clusters in iron-based MOFs, can be monosubstituted with various heteroatoms, such as Cr, Ni, Co, or Mn. Hence, heat treatment of MOFs consisting of well-defined mix metal structure was considered as a compelling method to produce nanoalloys enclosed inside porous carbons.

In this study, iron alloy nanoparticles-embedded porous carbons (FeM@PC) were fabricated by bimetallic MOFs-templated synthesis and applied to electrocatalytic oxygen evolution and reduction reactions in KOH_{aq.} solution. First, primary studies were conducted to optimize the pyrolysis step on a monometallic iron-based MOF. Next, influences of crystalline and chemical structures of the parent MOFs on the structure and reactivity of Fe@PC were inquired by heat treatment of various iron-based MOFs. MIL-126(Fe) was determined to be the best template due to its SBU structure and linkers. Furthermore, FeM@PC (M = Cr, Ni, Co, Mn) were successfully fabricated by pyrolysis of MIL-126(FeM), where MIL-126(FeM) were bimetallic MOFs constructed from ligand exchange process of preassembled clusters [Fe₂MO(CH₃COOH)₆(H₂O)₂OH], which assured the good dispersity and control over the amount of second metal. All materials were characterized and deposited on glassy carbon. Their electrocatalytic activity for oxygen evolution and oxygen reduction reactions was inquired in 0.1 M KOH_{aq.} solution.

Results and discussion

Conditions optimisation of the pyrolysis step

In this study, three different iron-based MOFs, MIL-126, MIL-88B and MIL-53, were used as precursors for the creation of Fe@PC composites. These iron-based MOFs were synthesized based on previous reported procedures. Typically, FeCl₃·6H₂O and the organic linker were mixed inside dimethylformamide (DMF) before being heated under solvothermal conditions at appropriate temperatures and times. Powder X-Ray Diffraction (PXRD) and N₂ adsorption-desorption isotherm analyses of the MOFs are shown respectively in Supporting Information Fig. S1 (a) and (b). The results fitted well with known values and confirmed the successful formation of the structures.

Preliminary studies focused on the optimization of the pyrolysis step. First experiments were carried out by heating MIL-126 under inert Argon (Ar) atmosphere at 700°C for several different pyrolysis time, which demonstrated that 2

hours was sufficient to obtain graphitization of carbon and iron particles. Further investigations were executed by varying the temperature to 500 and 900°C for 2 hours. The obtained powders were called MIL-126-T where T is the temperature in degree Celsius. In the case of pyrolysis at 700°C, the yield of the process was found to be around 30%.

As observed by PXRD analysis in Fig. 1 (a), MIL-126 characteristic peaks disappeared after all thermal treatments, confirming the destruction of the MOF. Pyrolysis at 500°C produced Fe₃O₄, and the oxygen source was considered to be the carboxylic acid groups of the linkers. Higher temperature, 700°C and 900 °C, enabled the creation of graphite, α-Fe⁰, and Fe₃C, as proved by the apparition of their respective peaks at 27°, 45°, and 42°/43°. Thermal treatment at 900°C led to higher crystalline particles than 700°C. N₂ adsorption-desorption analyses of MIL-126-T are shown in Fig. S2 (a) of Supporting Information. Aside from MIL-126-500, the composites displayed type IV N₂ adsorption-desorption isotherms, typical of mesoporous structure. Brunauer–Emmett–Teller (BET) analyses revealed lower surface area than parent-MOFs since the 3-dimensional structures were destroyed; but still higher compared to common carbon materials such as graphene or graphitic carbon nitride. Porosity and high surface area are important properties for catalysts since they assure good mass transport as well as efficient contact between substrates and active sites.

LSV analysis in 0.1M KOH_{aq.} solution of the MIL-126-T casted on glassy carbon was carried out under Ar atmosphere to study the efficiency of the composites for WOR (Fig. 1. (b)). MIL-126-500 displayed poor activity with an onset potential determined to be at 2.1 V vs RHE and did not attain sufficient current density in the range studied. On the contrary, 10 mA cm⁻² current density was achieved at 2.0 V for MIL-126-700, which proved that Fe⁰ or Fe₃C actively promoted WOR, unlike iron oxide. In comparison, MIL-126-900 achieved the same current density, but with a 30 mV more anodic overpotential. The higher electrocatalytic activity of MIL-126-700 was

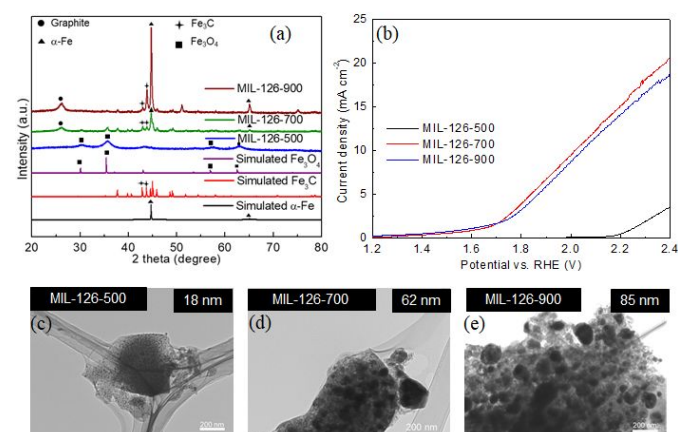


Fig. 1 (a) PXRD patterns of MIL-126 carbonized at different temperature and simulated reference structure, (b) LSV curves of MIL-126-T at a scan rate of 10 mV/s in 0.1 M KOH under Ar atmosphere. TEM images of (c) MIL-126-500, (d) MIL-126-700 and (e) MIL-126-900. The corresponding average size of nanoparticles is included in the onset on the upper right part of the image.

unexpected since the composite synthesized at 900°C exhibited better crystallinity. The answer was found in the diameter of the iron nanoparticles. Fig 1 (c)-(e) show Transmission Electron Microscopy (TEM) images of MIL-126-T. MIL-126-700 exhibited nanoparticles with an average size of 62 nm compared to 85 nm for 900°C. At equal quantity of metal, smaller nanoparticles often lead to better catalytic activity due to an increase of highly reactive atoms on faces, edges and corners. On the other hand, although the smallest nanoparticles with a mean size of 18 nm were observed in MIL-126-500, it was outside the discussion because these particles formed Fe₃O₄ phase that were not effective for WOR. Therefore, pyrolysis at 700°C for 2 hours was determined to be the best process. It was deemed to be the minimal temperature for formation of active sites and reduced phenomenon of aggregation caused by coalescence or Ostwald ripening occurring at higher temperature.

Effect of linker and inorganic cluster

To obtain a better insight of the structural factors of MOFs inducing the formation of Fe, Fe₃C and graphite, MIL-88B and MIL-53 underwent pyrolysis in the same conditions. MIL-88B is built from trinuclear cluster linked together through terephthalic acid. Thus, possessing a carbon content lower than MIL-126 composed of trinuclear cluster and biphenyl dicarboxylic acid (BPDC). As for MIL-53, the SBU is greatly different from the two previous MOFs, instead of trinuclear cluster, MIL-53 is composed of octahedral Fe³⁺ ions connected together by μ₂-OH groups forming a one-dimensional chain.

First, the average size of the Fe particles was inquired by TEM. It was discovered that MIL-88B and MIL-53 produced larger Fe particles than MIL-126 after carbonization. As shown in Fig. 2 (a)-(c), it was determined the average size slightly increased from 62 nm for MIL-126-700 to 77 nm for MIL-88B-700 and excessively surged in the case of MIL-53-700. The particles measured in MIL-53-700 and MIL-88B-700 were determined to be Fe⁰ since it was the only structure observed

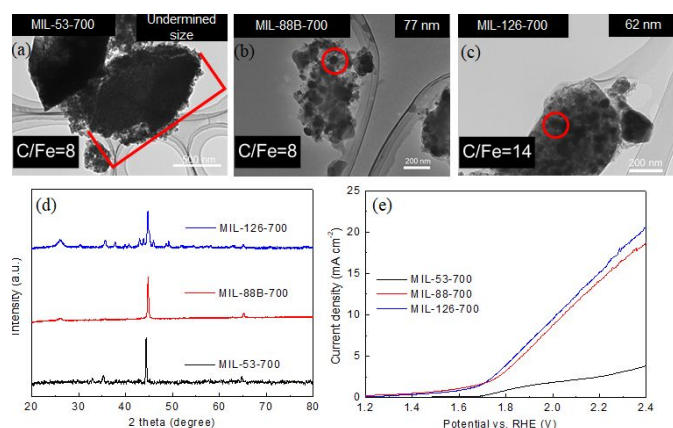


Fig. 2 TEM images of (c) MIL-53-700, (d) MIL-88B-700 and (e) MIL-126-700, the red sign displayed pinpointed Fe particle. (d) PXRD patterns of carbonized MOFs at 700°C for 2 hours, the Fe⁰ peak was observed in all materials whereas Fe₃C could be detected only from MIL-126-derived composites, this emphasizes the importance of carbon content when creating carbide, and (e) electrochemical performances of the iron-based MOFs-derived composites for OER at a scan rate of 10 mV/s in 0.1 M KOH under Ar atmosphere.

in PXRD patterns displayed in Fig. 2 (d). In Supporting Information Fig. S2 (b) are shown the N₂ adsorption-desorption isotherms of MIL-126-, MIL-88B- and MIL-53-derived composites. They all exhibited type IV isotherms, distinctive of mesoporous structure. Compared to MIL-88B-700 and MIL-53-700, MIL-126-700 retained a higher specific surface area, attributed to the use of BPDC linker compared to terephthalic acid.

Electrochemical performances of MIL-126-, MIL-88B- and MIL-53-derived composites for WOR were inquired by LSV measurements. The obtained curves are shown in Fig. 2 (e), and clearly, bigger Fe⁰ particles caused lower electrocatalytic performances for WOR, which correlated with precedent results. Aggregation of the nanoparticles was attributed to two factors: first, the smaller size of terephthalic acid compared to BPDC. The longer linker, BPDC, enabled a better spatial segregation of the Fe₃O clusters. The second factor was determined to be the chain structure of the SBU of MIL-53 that easily promoted sintering of iron particles during pyrolysis since the iron cations are connected together. Fe₃C and graphite peaks were not observed in MIL-88B- and MIL-53-derived composites. The results imply that high C/Fe molar ratio is a crucial factor in the creation of carbides and crystallization of graphite. Although Fe₃C was absent of MIL-88B-700, it still exhibited activity for WOR, hence it was determined that the active site for this reaction was Fe⁰. In overall, the results demonstrated that the SBU structure and choice of linker are of fundamental importance when preparing metal particles-embedded porous carbons materials. MIL-126 proved to be the best template owing to the long linkers between each trinuclear clusters.

Alloying effect on Fe nanoparticles

In order to furthermore increase the activity of composites, alloying of iron was attempted by thermal treatment of heterometallic MOFs. Instead of direct solvothermal synthesis, employing preassembled clusters was favoured in the creation of bimetallic MIL-126. When introducing a second metal in direct synthesis, multiple issues can potentially occur because of the difference in thermodynamics, kinetics and diffusivity of the metal salts. Variations in reactivity of precursors can lead to core-shell like structures, gradient in concentration of metal or in the worst case, the appearance of another phase inside the structure. At the molecular level, the existence of multiple SBUs cannot be ruled out neither. To dismiss those problems, utilizing pre-synthesized bimetallic cluster followed by ligand exchange to create the three-dimensional MOFs is considered as a promising process³²⁻³⁵ (Fig. 3). The synthesis of Fe₂MO(CH₃COOH)₆ where M = Cr³⁺, Mn²⁺, Co²⁺ or Ni²⁺ was carried out by mixing iron nitrate, metal nitrate and sodium acetate in water. Due to the low solubility of trinuclear acetate complexes in water, the clusters were easily collected by filtration and used for MOFs synthesis. PXRD patterns and N₂ adsorption-desorption isotherms of MIL-126(FeM) synthesized from ligand exchange are shown in Supporting Information Fig. S1 (c) and (d), respectively. No

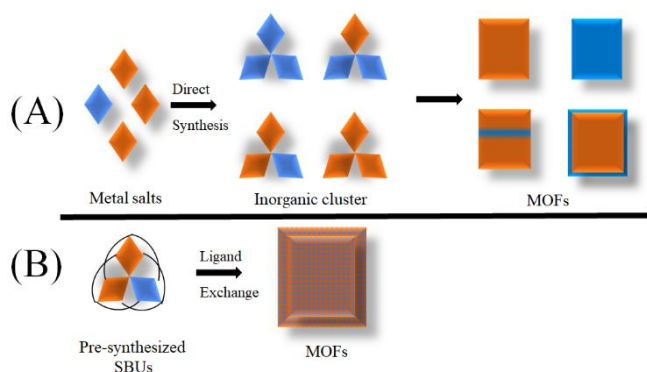


Fig. 3 Fabrication of MOFs employing (A) Direct synthesis with multiple metal sources and possible issues emerging from this method, such as the formation of different SBUs at the molecular level and the creation of crystals with different chemical and crystalline structures, (B) preassembled SBUs to control the content of dopant and its dispersity.

differences were observed in the PXRD peaks compared to MIL-126 synthesized by direct synthesis, and type I isotherms were also observed, proving the successful formation of MIL-126 structure through this method. The metal ratio Fe/M was conserved between the clusters and the corresponding MOFs as determined by ICP-MS analysis.

PXRD patterns of pyrolyzed bimetallic MOFs, henceforth called MIL-126(FeM)-700, are shown in Fig. 4. The main peak of Fe⁰ slightly shifted in all samples compared to pure Fe@PC. In the case of MIL-126(FeNi)-700, heat treatment produced Fe–Ni alloys of the face-centered cubic (FCC) structure³⁶ as detected by the apparition of two peaks at 44° and 50°. Slight shift at lower angle for Fe–Mn^{37,38} or higher angle for Fe–Co³⁹ were observed confirming the body-centered cubic (BCC) structure of the respective alloys. For Fe–Cr alloys, determination of the structure could not be achieved since σ (body-centered tetragonal) and α (BCC) peaks are too close to each other.⁴⁰ Interestingly, only Cr- and Mn-doped composites exhibited the Fe₃C structure. Carbidization of d-block transition metals tends to gradually become harder from left to right in the periodic table due to the M–C bonds energy being reduced.³⁹ Because iron is substituted by Co or Ni, synthesis of Fe₃C structure becomes more difficult at same carbon content. As seen in Supporting Information Fig. S2 (c), the N₂

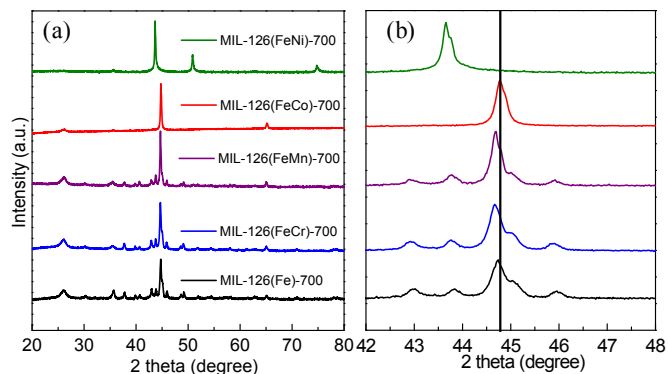


Fig. 4 (a) PXRD patterns of MIL-126(FeM)-700, and (b) zoom in between 42°–48°. A clear shift of the Fe⁰ main peak structure can be observed, attesting the successful alloys formation.

adsorption-desorption isotherms of MIL-126(FeM)-700 all displayed the expected type IV isotherms defining mesoporous materials. The specific surface area determined by BET analyses were of the same order as those detailed previously. TEM images of MIL-126(FeM)-700 composites were taken to confirm the size of the nanoparticles and are shown in Fig. S3. All composites displayed alloy particles with an average size centered around 50 nm, hence, effect of nanoparticle size on the difference in electroactivity can be considered as minimal.

LSV curves analyses for MIL-126(FeM)-700 are shown in Fig. 5 (a), and it was determined that all composites promoted WOR with better activity than MIL-126(Fe)-700. The composites achieved 10 mA cm⁻² following the order in needed overpotential: Co < Cr < Mn < Fe = Ni. Electrochemical impedance spectroscopy was employed to qualitatively estimate the conductivity between the electrocatalysts and the electrolyte. In Fig. 5 (b) are presented the Nyquist plots obtained at low frequency, they revealed an increase in the radius of the semi-circle following the trend Co < Ni < Cr < Mn < Fe, demonstrating lower resistivity of the alloy compared to pure metal. On the whole, MIL-126(FeCo)-700 exhibited the lowest overpotential, achieving 10 mA current density at 1.79 V vs RHE, this represented a 0.21 mV cathodic shift compared to MIL-126(Fe)-700. The large overpotential to achieve 10 mA of current density for MIL-126(FeNi)-700 was hypothesized to be caused either by its different crystalline structure (FCC) or by the carbon matrix state. While graphite conductivity is not exceptional, it is still higher than amorphous carbon. But in the case of MIL-126(FeNi)-700, the peak at 27° characteristic of graphite was absent. Consequently, it was difficult for the electron to flow back into the glassy carbon under these conditions. Stability of MIL-126(FeCo)-700 was then inquired by LSV before and after 1000 cycles (Fig. 5 (c)), and no change was observed in its electroactivity, attesting that the material

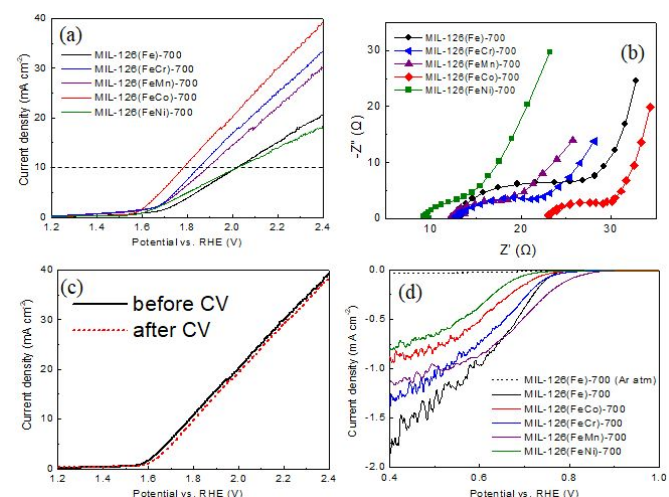


Fig. 5 (a) LSV curves of MIL-126(FeM)-700 for OER at a scan rate of 10 mV/s in 0.1 M KOH under Ar atmosphere. (b) Nyquist plot of MIL-126(FeM)-700 measured at 1.3 V vs RHE, (c) recyclability test of MIL-126(FeCo)-700 after 1000 cycles, and (d) LSV curves of MIL-126(FeM)-700 for ORR at a scan rate of 10 mV/s in 0.1 M KOH under O₂ atmosphere. The dotted line in (d) shows the result for MIL-126(FeM)-700 under Ar atmosphere.

was stable in 0.1 M KOH aqueous solution under oxidative conditions.

Since carbides are also well-known for their reductive properties,^{41–43} oxygen reduction reaction (ORR) activity of the materials was also inquired. As seen in Fig. 5 (d), no reduction peak could be observed under Ar atmosphere when employing MIL-126(Fe)-700 as electrocatalyst. After bubbling the solution with O₂, a peak appeared at 0.8 V vs RHE, which demonstrates the catalytic activity of the material for ORR. MIL-126(FeMn)-700 exhibited the lowest overpotential, with ORR onset potential appearing at 0.88 V vs RHE compared to approximately 0.8 V vs RHE for other composites. The overall activity trend obtained clearly demonstrated that carbides efficiently promote ORR, as proved by the topping efficiency of MIL-126(Fe)-700, MIL-126(FeCr)-700 and MIL-126(FeMn)-700, which are the three composites where Fe₃C could be detected. Considering that high carbon content is necessary for the creation of carbide and that doping with nitrogen has been recognized as an impactful method to increase the activity for ORR, azobenzene dicarboxylic acid or bipyridine dicarboxylic acid are promising linkers that might unlock even more active FeM@PC after pyrolysis of respective MOFs.

Conclusions

To conclude, pyrolysis of iron-based MOFs was carried under Ar atmosphere to create metal nanoparticles confined inside porous carbons (Fe@PC). After optimizing the experimental conditions, MIL-126 was determined to be the best template for the creation of Fe@PC due to its long linker, high carbon content and array of trinuclear cluster. Alloyzation of the iron nanoparticles succeeded by pyrolysis of bimetallic MOFs built from pre-synthesized Fe₂MO(CH₃COOH)₆(H₂O)₂OH (M = Cr, Mn, Ni, Co) SBUs. The Co- and Mn-doped alloy nanoparticle-embedded porous carbons respectively exhibited the best activity for WOR and ORR, each of them lowering the overpotential needed for the reactions to efficiently occur. Structural and morphological properties of the components were found to be essential, with size of the metal nanoparticles and crystalline state of the carbon matrix being the most crucial one. Future research can be orientated in the synthesis of trimetallic MOFs and MOF-derived compounds seeing how the FeCrMO(CH₃COOH)₆ cluster has been reported in the past⁴⁴. Instead of focusing on carbide, the synthesis of phosphide,¹⁹ sulphide and selenide⁴⁵ as well as nitrogen doping of the carbon matrix⁴⁶ are also contemplated as promising methods to create better catalysts.

Experimental

Materials

O₂ and Ar were purchased from Nihon Helium Company. Fe(NO₃)₃ · 9H₂O, Cr(NO₃)₃ · 9H₂O, Ni(NO₃)₂ · 6H₂O, Mn(NO₃)₂ · 6H₂O, Co(NO₃)₂ · 6H₂O, sodium acetate trihydrate, N,N-dimethyl formamide (DMF), Methanol (MeOH), acetic acid, potassium hydroxide (KOH), ethanol, acetone and

water were acquired from Nacalai tesque. 4,4'-Biphenyldicarboxylic acid (BPDC), terephthalic acid (BDC) were bought from Tokyo Kagaku Kenkyuusho.

Equipment and analysis

Specific surface area was estimated from the amount of N₂ adsorption collected with a BEL-SORP mini (Microtrac BEL) at 77 K using the BET (Brunauer–Emmett–Teller) equilibrium equation. The MOFs were vacuumed at 373 K for 1 hour before analysis. Standard ϑ -2 ϑ X-ray diffraction (PXRD) data were recorded on a Rigaku SmartLab X-ray diffractometer using Cu K α radiation (λ = 1.5406 Å). Transmission electron microscopy (TEM) images were obtained with a JEM-2000FX operating under 200 kV accelerating voltage.

Electrochemical cell

The working electrodes were fabricated following a simple casting method. 16 mg of powder was dispersed in acetone (180 μ L), ethanol (180 μ L), and Nafion[®] dispersion solution (40 μ L). After sonication, 20 μ L of the mixture was drop-casted on the glassy carbon electrodes and dried in air at room temperature.

Electrochemical measurements were performed using a three-electrodes system. The working electrode were either the Fe@PC or FeM@PC-deposited on glassy carbon, the counter and reference electrodes were respectively platinum foil and Ag/AgCl. All analyses were executed in 0.1M KOH aqueous solution under Ar or O₂ bubbling.

Synthetic procedure

Preparation of MIL-126 (direct synthesis)

FeCl₃ · 6H₂O (270 mg, 1mmol) and 2,4'-biphenyldicarboxylic acid (242 mg, 1mmol) were dissolved in 5 DMF (5 mL). The solution was poured in a Teflon lined autoclave and heated at 473 K for 12 hours. After cooling down, the mixture was centrifugated and washed with MeOH multiple times. The obtained powder was stirred inside 20 mL MeOH for 16 hours to remove the unreacted salts, linkers and DMF.

Preparation of MIL-88B (direct synthesis)

FeCl₃ · 6H₂O (270 mg, 1mmol) and terephthalic acid (166 mg, 1 mmol) were dissolved in DMF (10 mL) and 2M NaOH (0.4 mL). The solution was poured in a Teflon lined autoclave and heated at 373 K for 12 hours. After cooling down, the mixture was centrifugated and washed with MeOH multiple times. The obtained powder was stirred inside 20 mL MeOH for 16 hours to remove the unreacted salts, linkers and DMF.

Preparation of MIL-53 (direct synthesis)

FeCl₃ · 6H₂O (540 mg, 2mmol) and terephthalic acid (332 mg, 2 mmol) were dissolved in 5 DMF (40 mL). The solution was poured in a Teflon lined autoclave and heated at 473 K for 48 hours. After cooling down, the mixture was centrifugated and washed with MeOH multiple times. The obtained powder was stirred inside 20 mL MeOH for 16 hours to remove the unreacted salts, linkers and DMF.

Preparation of [Fe₃O(CH₃COOH)₆(H₂O)₃OH] (Fe₃O cluster)

Iron (III) nitrate nonahydrate (4.04 g, 10 mmol) was dissolved in 25 mL of water. In another beaker, sodium acetate trihydrate (12.76 g, 0.1 mol) was dissolved in 25 mL of water. The two solutions were mixed and stirred for 24 hours at room temperature where crystallization occurred. The cluster was filtrated and intensively washed with distilled water and a bit of ethanol. Finally, the powder was dried under vacuum at room temperature.

Preparation of [Fe₂MO(CH₃COOH)₆(H₂O)₃OH] (FeMO cluster)

where M= Ni²⁺, Co²⁺ and Mn²⁺

Iron (III) nitrate nonahydrate (1.3 g, 3.3 mmol) and the second metal nitrate (0.17 mol) were dissolved in 11.6 mL of water. In another beaker, sodium acetate trihydrate (7 g, 0.5 mol) was dissolved in 11.6 mL of water. The two solutions were mixed and stirred for 24 hours at room temperature where crystallization occurred. The cluster was filtrated and intensively washed with distilled water. Finally, the powder was dried under vacuum at room temperature.

Preparation of [Fe₂CrO(CH₃COOH)₆(H₂O)₃OH] (Fe₂Cr cluster)

Iron (III) nitrate nonahydrate (4.04 g, 10 mmol) and chromium nitrate nonahydrate (2g, 5 mmol) were dissolved in 5 mL of hot water. In another beaker, sodium acetate trihydrate (4.08 g, 30 mmol) was dissolved in 5 mL of hot water. The two solutions were mixed and stirred for 24 hours at room temperature where crystallization occurred. The cluster was filtrated and intensively washed with distilled water and a bit of ethanol. Finally, the powder was dried under vacuum at room temperature.

Preparation of MIL-126(Fe) (ligand exchange)

Fe₃O cluster (200 mg) and 4,4'-Biphenyldicarboxylic acid (0.242 g) were dispersed in DMF (6 mL). After transposition of the mixture in a Teflon lined autoclave, it was heated at 423 K for 12 hours. The MOF was collected by filtration and washed 3 times with methanol. The obtained powder was dispersed in 80 mL of MeOH and stirred overnight before being filtrated again.

Preparation of MIL-126(FeM) (ligand exchange) where M= Ni²⁺, Co²⁺, Mn²⁺ and Cr³⁺

The same method described above was applied with some arrangements. For bimetallic MOFs, Fe₂M cluster (200 mg) and 4,4'-Biphenyldicarboxylic acid (0.242 g) were dispersed in DMF (8 mL) and acetic acid (1 mL) before the solvothermal reaction at 423 K for 12 hours. MIL-126(FeM) powders were centrifugated, washed with MeOH and dispersed in 80 mL of fresh MeOH before being stirred overnight. After filtration, the MOFs were conserved at room temperature under vacuum.

Pyrolysis of the MOFs

Pyrolysis of the MOFs was accomplished in a tube furnace. Before heating, the equipment was flowed with Argon flow (60

mL/min) for 15 minutes. The ramp temperature increased at a fixed rate of 5 K/min before being kept at X°C (X = 500°C, 700°C and 900°C) for 2 hours. The powders were recovered after cooling down until room temperature.

Conflicts of interest

There are no conflicts to declare.

Acknowledgements

This work was financially supported by JST ACCEL, Japan (Grant No. JPMJAC1302), by the Grants-in-Aid for Scientific Research (KAKENHI) from the Ministry of Education, culture, Sports, Science and Technology of Japan (No. 15K17903, 15K13820 and 18K14305) and by the Global Research Program of the National Research Foundation of Korea (NRF) funded by the Ministry of Education, Science and Technology (MEST), Korea (Grant No. 2010-00339).

Notes and references

- 1 C. C. L. McCrory, S. Jung, I. M. Ferrer, S. M. Chatman, J. C. Peters and T. F. Jaramillo, *J. Am. Chem. Soc.*, 2015, **137**, 4347–4357.
- 2 T. Audichon, T. W. Napporn, C. Canaff, C. Morais, C. Comminges and K. B. Kokoh, *J. Phys. Chem. C*, 2016, **120**, 2562–2573.
- 3 V. R. Stamenkovic, B. S. Mun, M. Arenz, K. J. J. Mayrhofer, C. A. Lucas, G. Wang, P. N. Ross and N. M. Markovic, *Nat. Mater.*, 2007, **6**, 241–247.
- 4 Z. Pu, I. S. Amiinu, Z. Kou, W. Li and S. Mu, *Angew. Chemie - Int. Ed.*, 2017, **56**, 11559–11564.
- 5 N. Mamaca, E. Mayousse, S. Arrii-Clacens, T. W. Napporn, K. Servat, N. Guillet and K. B. Kokoh, *Appl. Catal. B Environ.*, 2012, **111–112**, 376–380.
- 6 I. Roger, M. A. Shipman and M. D. Symes, *Nat. Rev. Chem.*, DOI:10.1038/s41570-016-0003.
- 7 M. Gong, Y. Li, H. Wang, Y. Liang, J. Z. Wu, J. Zhou, J. Wang, T. Regier, F. Wei and H. Dai, *J. Am. Chem. Soc.*, 2013, **135**, 8452–8455.
- 8 A. J. Esswein, Y. Surendranath, S. Y. Reece and D. G. Nocera, *Energy Environ. Sci.*, 2011, **4**, 499–504.
- 9 L. Zhang, J. Xiao, H. Wang and M. Shao, *ACS Catal.*, 2017, **7**, 7855–7865.
- 10 Y. Xu, M. Kraft and R. Xu, *Chem. Soc. Rev.*, 2016, **45**, 3039–3052.
- 11 F. M. Toma, A. Sartorel, M. Iurlo, M. Carraro, P. Parisse, C. MacCato, S. Rapino, B. R. Gonzalez, H. Amenitsch, T. Da Ros, L. Casalis, A. Goldoni, M. Marcaccio, G. Scorrano, G. Scoles, F. Paolucci, M. Prato and M. Bonchio, *Nat. Chem.*, 2010, **2**, 826–831.
- 12 X. Yue, S. Huang, J. Cai, Y. Jin and P. K. Shen, *J. Mater. Chem. A*, 2017, **5**, 7784–7790.
- 13 S. J. Yang, T. Kim, J. H. Im, Y. S. Kim, K. Lee, H. Jung and C. R. Park, *Chem. Mater.*, 2012, **24**, 464–470.

Journal Name

ARTICLE

- 14 W. Chaikittisilp, K. Ariga and Y. Yamauchi, *J. Mater. Chem. A*, 2013, **1**, 14–19.
- 15 K. Shen, X. Chen, J. Chen and Y. Li, *ACS Catal.*, 2016, **6**, 5887–5903.
- 16 W. Li, X. Wu, N. Han, J. Chen, X. Qian, Y. Deng, W. Tang and Y. Chen, *Sensors Actuators, B Chem.*, 2016, **225**, 158–166.
- 17 M. Huang, K. Mi, J. Zhang, H. Liu, T. Yu, A. Yuan, Q. Kong and S. Xiong, *J. Mater. Chem. A*, 2017, **5**, 266–274.
- 18 B. Liu, H. Shioyama, H. Jiang, X. Zhang and Q. Xu, *Carbon N. Y.*, 2010, **48**, 456–463.
- 19 L. Yan, L. Cao, P. Dai, X. Gu, D. Liu, L. Li, Y. Wang and X. Zhao, *Adv. Funct. Mater.*, 2017, **27**, 1–10.
- 20 W. Zhang, X. Jiang, Y. Zhao, A. Carné-Sánchez, V. Malgras, J. Kim, J. H. Kim, S. Wang, J. Liu, J. Sen Jiang, Y. Yamauchi and M. Hu, *Chem. Sci.*, 2017, **8**, 3538–3546.
- 21 S. L. Zhang, B. Y. Guan and X. W. D. Lou, *Small*, 2019, **15**, 1805324.
- 22 H. J. Lee, S. Choi and M. Oh, *Chem. Commun.*, 2014, **50**, 4492–4495.
- 23 P. Zhao, X. Hua, W. Xu, W. Luo, S. Chen and G. Cheng, *Catal. Sci. Technol.*, 2016, **6**, 6365–6371.
- 24 J. Wei, Y. Liang, Y. Hu, B. Kong, G. P. Simon, J. Zhang, S. P. Jiang and H. Wang, *Angew. Chemie - Int. Ed.*, 2016, **55**, 1355–1359.
- 25 Y. Chen, S. Ji, Y. Wang, J. Dong, W. Chen, Z. Li, R. Shen, L. Zheng, Z. Zhuang, D. Wang and Y. Li, *Angew. Chemie - Int. Ed.*, 2017, **56**, 6937–6941.
- 26 A. Banerjee, R. Gokhale, S. Bhatnagar, J. Jog, M. Bhardwaj, B. Lefez, B. Hannyer and S. Ogale, *J. Mater. Chem.*, 2012, **22**, 19694–19699.
- 27 C. Li, Q. Hu, Y. Li, H. Zhou, Z. Lv, X. Yang, L. Liu and H. Guo, *Sci. Rep.*, 2016, **6**, 1–8.
- 28 E. Kim and M. Yoon, *J. Porous Mater.*, 2015, **22**, 1495–1502.
- 29 T. A. Wezendonk, Q. S. E. Warringa, V. P. Santos, A. Chojecki, M. Ruitenbeek, G. Meima, M. Makkee, F. Kapteijn and J. Gascon, *Faraday Discuss.*, 2017, **197**, 225–242.
- 30 A. K. Singh and Q. Xu, *ChemCatChem*, 2013, **5**, 652–676.
- 31 C. Wang, D. Li, M. Chi, J. Pearson, R. B. Rankin, J. Greeley, Z. Duan, G. Wang, D. Van Der Vliet, K. L. More, N. M. Markovic and V. R. Stamenkovic, *J. Phys. Chem. Lett.*, 2012, **3**, 1668–1673.
- 32 D. Feng, K. Wang, Z. Wei, Y. P. Chen, C. M. Simon, R. K. Arvapally, R. L. Martin, M. Bosch, T. F. Liu, S. Fordham, D. Yuan, M. A. Omary, M. Haranczyk, B. Smit and H. C. Zhou, *Nat. Commun.*, DOI:10.1038/ncomms6723.
- 33 L. Peng, M. Asgari, P. Mieville, P. Schouwink, S. Bulut, D. T. Sun, Z. Zhou, P. Pattison, W. Van Beek and W. L. Queen, *ACS Appl. Mater. Interfaces*, 2017, **9**, 23957–23966.
- 34 C. Serre, F. Millange, S. Surblé and G. Férey, *Angew. Chemie - Int. Ed.*, 2004, **43**, 6286–6289.
- 35 M. J. Kalmutzki, N. Hanikel and O. M. Yaghi, *Sci. Adv.*, DOI:10.1126/sciadv.aat9180.
- 36 P. Jing, M. Liu, Y. Pu, Y. Cui, Z. Wang, J. Wang and Q. Liu, *Sci. Rep.*, 2016, **6**, 1–9.
- 37 Y. Yang, Z. Shen, L. Liu, Y. Zhang, C. Song and Q. Zhai, *TMS 2015 144th Annu. Meet. Exhib.*, 2016, **18**, 1457–1463.
- 38 N. Safaie, M. Khakbiz, S. Sheibani and P. S. Bagha, *Procedia Mater. Sci.*, 2015, **11**, 381–385.
- 39 F. Sánchez-De Jesús, A. M. Bolarín-Miró, C. A. Cortés Escobedo, G. Torres-Villaseñor and P. Vera-Serna, *J. Metall.*, 2016, **2016**, 1–8.
- 40 T. R. Gao, S. P. Hao, S. M. Zhou and L. Sun, *J. Appl. Phys.*, 2006, **100**, 073909.
- 41 W. F. Chen, J. T. Muckerman and E. Fujita, *Chem. Commun.*, 2013, **49**, 8896–8909.
- 42 M. Chen, J. Liu, W. Zhou, J. Lin and Z. Shen, *Sci. Rep.*, 2015, **5**, 1–10.
- 43 X. Ma, H. Meng, M. Cai and P. K. Shen, *J. Am. Chem. Soc.*, 2012, **134**, 1954–1957.
- 44 A. B. Blake, A. Yavari, W. E. Hatfield and C. N. Sethulekshmi, *J. Chem. Soc. Dalton Trans.*, 1985, 2509–2520.
- 45 S. Anantharaj, S. R. Ede, K. Sakthikumar, K. Karthick, S. Mishra and S. Kundu, *ACS Catal.*, 2016, **6**, 8069–8097.
- 46 Z. Y. Wu, X. X. Xu, B. C. Hu, H. W. Liang, Y. Lin, L. F. Chen and S. H. Yu, *Angew. Chemie - Int. Ed.*, 2015, **54**, 8179–8183A.